

Primljen / Received: 2.6.2021.

Ispravljen / Corrected: 1.6.2022.

Prihvaćen / Accepted: 31.7.2022.

Dostupno online / Available online: 10.11.2022.

# Numerical modelling of floating structure with coupled Eulerian–Lagrangian technique

## Authors:



Assoc.Prof. **Engin Gücüyen**, PhD. CE  
Manisa Celal Bayar University, Turkey  
Department of Civil Engineering  
[engin.gucuyen@cbu.edu.tr](mailto:engin.gucuyen@cbu.edu.tr)

Corresponding author



Assoc.Prof. **R. Tuğrul Erdem**, PhD. CE  
Manisa Celal Bayar University, Turkey  
Department of Civil Engineering  
[tugrul.erdem@cbu.edu.tr](mailto:tugrul.erdem@cbu.edu.tr)

Professional paper

**Engin Gücüyen, R. Tuğrul Erdem**

## Numerical modelling of floating structure with coupled Eulerian–Lagrangian technique

Floating structures are complex systems composed of superstructure, floating-mooring components, and anchors. In this study, the behaviours of a pontoon, which is used as a floating structure, and four mooring elements under different wave loading conditions were investigated. A numerical analysis of the coupled motions of the pontoon, mooring lines, and marine environment was performed. While the mooring lines were modelled as wire elements, the pontoon was modelled as a rigid body with six degrees of freedom. Wave loading conditions were represented using two different wave spectra. The first spectrum (Case I) was generated based on a single sinusoidal wave utilising the JONSWAP spectrum, whereas the second one (Case II) was generated based on a superimposed multi-sinusoidal wave. Time-varying motions of the pontoon and tensions of the mooring lines were determined based on the numerical analyses for Cases I and II. Critical values were determined using the results of both cases. The numerical solutions were based on bidirectional fluid–structure interaction (FSI) analysis. A fully non-linear free surface simulation was performed using the coupled Eulerian–Lagrangian (CEL) technique. Furthermore, numerical results were compared with the results obtained from analytical solutions of free surface elevations.

### Key words:

floating structure, fluid–structure interaction, finite elements analysis, coupled Eulerian–Lagrangian technique

Stručni rad

**Engin Gücüyen, R. Tuğrul Erdem**

## Numeričko modeliranje plutajuće konstrukcije primjenom spregnute Euler-Lagrangeove formulacije

Plutajuće konstrukcije složeni su sustavi sastavljeni od platforme (pontona), priveznih elemenata i konopa. U ovom radu istražuje se ponašanje pontona koji se koristi kao plutajuća konstrukcija i četiri privezna elementa pod utjecajem različitih uvjeta opterećenja valovima. Kombinirana analiza se numerički provodi između kretanja pontona, konopa za privez i morskog okoliša. Konopi za privez modelirani su kao mrežni elementi, a ponton je modeliran kao kruto tijelo sa šest stupnjeva slobode kretanja. Stanje opterećenja valovima predstavljeno je pomoću dva različita valna spektra. Prvi se spektar (slučaj I) generira iz jednog sinusoidnog vala korištenjem Jonswapovog spektra, drugi (slučaj II) se generira iz superponiranog višesinusoidnog vala. Vremenski promjenjivo kretanje pontona i napetosti konopa za privez određeni su numeričkom analizom za slučaj I i slučaj II. Na temelju rezultata oba slučaja određene su kritične vrijednosti. U numeričkim rješenjima primijenjena je dvosmjerna analiza interakcije fluid-konstrukcija (FSI). U analizi se provodi potpuno nelinearna simulacija slobodne površine pomoću tehnike spregnute Euler-Lagrangeove formulacije. Uz to, numerički rezultati uspoređeni su s rezultatima dobivenim analitičkim rješavanjem kota slobodnih površina.

### Ključne riječi:

plutajuća konstrukcija, interakcija fluida i konstrukcije, analiza konačnih elemenata, spregnuta Euler-Lagrangeova (CEL) formulacija

## 1. Introduction

Offshore structures can be floating or fixed objects on the sea bottom. Unlike fixed structures on the sea bottom, floating structures are not affected by the water depth and sea bottom effects. As they do not restrain sea flow, they exhibit an environmentalist attitude. In addition to these positive features, floating structures are easily installed and can be utilised in other locations. Moreover, they afford flexibility for future extensions; short time durations are needed for installation and a relatively low construction costs are incurred for large water depths and soft bed scenarios.

Floating structures have become prevalent as they can be used at any depth, that is, shallow water, transition zone, and deep water. A typical floating structure consists of a superstructure, floaters where the superstructure is placed, mooring lines fixing floaters to the ground, and anchors. The superstructure can be a truss system, a single pile, or another type of structure according to the intended purpose. Stability of the superstructure can be provided via three different approaches—without using floaters (i.e., only using mooring lines), with ballasts, and with pontoons.

Pontoons can be fully or partially submerged in water. In these two cases, pontoons can be used as mobile offshore bases [1], breakwaters [2, 3], wave energy generators [4, 5], floating net cages for fish breeding [6], bridges [7], offshore barrier structures [8], landing fields, entertainment areas, and piers. Adverse conditions due to prevalent usage are described in prior works [9, 10]. Pontoons have wide surfaces and a small thicknesses. Therefore, they may be vulnerable to stretching and bending under wave force effects. Moreover, fractures may develop owing to vertical displacements during strong storms [11].

Floating pontoons are complex structures that are affected by different load cases. The main environmental force affecting floating offshore structures is the wave force. Regular and irregular waves are considered in the behaviour modelling of wave loads. Lim and Kim [12] modelled the behaviour of a pontoon-type platform with ropes under the effect of irregular waves. Two methods were used to investigate the irregular wave, namely those based on extreme response amplitude and most likely extreme response profile. Cheng et al. [13] experimentally and numerically investigated the hydroelastic behaviour of a pontoon-type large structure in terms of porosity and submerged depth parameters. The FSI technique is utilised in the numerical model. The finite element method is used in the structural model, while the boundary element method is used in the wave model for irregular waves. Trubat et al. [14] experimentally and numerically investigated the surge, heave, and pitch motions and tensions of the moorings of the offshore floating structure. Although regular wave conditions were considered in the experiments, irregular waves were considered in the numerical analysis. Irregular waves were considered as superpositions of regular waves. Jin et al. [15] considered

regular and irregular wave models together. Structural analysis of a floating structure according to regular and irregular wave models was generated through hydroelastic analysis, and the behaviour of floaters was ultimately obtained. Similarly, fully coupled mooring–structure dynamics were simulated under regular waves that are generated from irregular waves by Howe et al. [16].

Owing to the mooring lines, floating structures can be utilised at any water depth. However, mooring lines are susceptible to failure. Therefore, the behaviour of these lines should be considered in the analyses. The use of different cable configurations have been reported in the literature, such as the catenary mooring system and the taut, semi-taut, and hybrid mooring systems with buoys and catenary lines. Yuan et al. [17] have investigated the motion responses of a semi-submersible platform moored by the hybrid mooring system, and the results with those of the taut mooring system. Chung et al. [18] used chain-moorings to study the performance simulation of coupled hull–mooring–riser systems by using Abaqus software. Qiao et al. [19] modelled a slack–taut mooring system to investigate the motion responses of the mooring line under hydrodynamic load by using finite element analysis.

As the motions of the floating elements can be affected by the mooring system, a coupled analysis of the motions of the floating elements and mooring forces is necessary. Wiegard et al. [20] performed the interaction analysis of the floaters and mooring lines. Thus, the motions of these elements were numerically modelled. Displacement and stress values of the superstructure were also obtained. Chen et al. [21] analysed the interaction of a pontoon-type floating structure with the mooring lines according to degree of freedom. Time-varying force values on the mooring lines were obtained as well as the motion of the pontoon. Ji et al. [22] experimentally and numerically modelled the floating type breakwater and mooring lines. Sway, heave, and roll motions of the breakwater were obtained under different wave conditions via a coupled Eulerian–Lagrangian numerical procedure.

FSI analysis has been employed to determine the dynamic behaviour of offshore structures. The analysis is unidirectional when the force transfer occurs from the fluid to the structure only. However, in case of bidirectional analysis, the force is transferred from the fluid and the displacement is transferred from the structure. Finite element analysis is applied for both analyses. Finite element-supported FSI analysis can be accomplished using either the Eulerian technique [23] or the Lagrangian technique [24]. Nevertheless, both techniques can also be used in arbitrary Lagrangian–Eulerian (ALE) [25, 26] and coupled Eulerian–Lagrangian (CEL) [27] analyses. Abaqus finite element software is widely used in interaction modelling [28]. In ALE and CEL analyses, the structure and the fluid are modelled by using Lagrangian and Eulerian techniques, respectively. Thus, there is no need to define the interaction surface and to use co-simulation when Lagrangian and Eulerian techniques are utilised together. Moreover, high structural–element distortions

that occur in the ALE technique could lead to unrealistic results and could even crash on-going simulations [29]. The CEL technique, which is implemented in the software Abaqus and uses an explicit time integration scheme, is a large-deformation finite element method intended to address the deficiencies of the pure Lagrangian and Eulerian techniques [30]. CEL is composed of an Eulerian mesh symbolising the volume where the Eulerian material flows and interacts with the Lagrangian part. The fluid motion in CEL is defined by using the traditional Eulerian technique, wherein the numerical grid is fixed in space while the fluid flows through the grid. The inflatable structure, however, is defined using the traditional Lagrangian description of motion and discretised using the Lagrange method wherein the numerical grids moves and deforms with the material [31]. A literature review reveals that modelling of the dynamic behaviour of pontoon-type offshore structures can be realised via analytical [32], numerical [33, 34] and experimental [35] procedures.

This study aimed to numerically investigate the dynamic behaviour of pontoon-type structure and mooring lines under different wave loading conditions. A CEL technique, using Abaqus software, was used for numerical analysis. The structure was modelled using the Lagrangian technique, while the marine environment was modelled using the Eulerian technique. Sway, heave, and pitch motions of the structure and tensions of the moorings were obtained for different wave loading conditions. Thus, the effect of these conditions on the floating structure was investigated, and it was demonstrated that the design of floating structure comprehensively by numerical modelling yields more critical results. Moreover, the advantages of the CEL technique over the pure Lagrangian technique was demonstrated in terms of point-element numbers and solution steps for such type of structures.

## 2. Structural and environmental models

In this study, three dimensional moored floating structures and slender mooring lines coupled with the marine environment were investigated. The coupled system is shown in Figure 1. The mooring system consists of four mooring lines. The top ends of the mooring lines are connected to the structure, and the other ends are fixed to the sea bed. The numerical model has 18 m x 72 m base dimensions with a height of 20 m. The width of the computational domain in the finite element model is set as six times the width of the pontoon ( $6 \times B$ ), and the length of the domain is nine times the pontoon length ( $9 \times L_p$ ). In addition, the height value is ten times the pontoon height ( $10 \times h_p$ ).

**Table 1. Geometrical parameters of structure and mooring lines**

Parameters of the structure				Parameters of mooring lines			
$h_p$ [m]	$B$ [m]	$L_p$ [m]	$h_d$ [m]	$l$ [m]	$\theta$ [°]	$s/l$	$r$ [m]
2	3	8	0.80	28	30	50	0.05

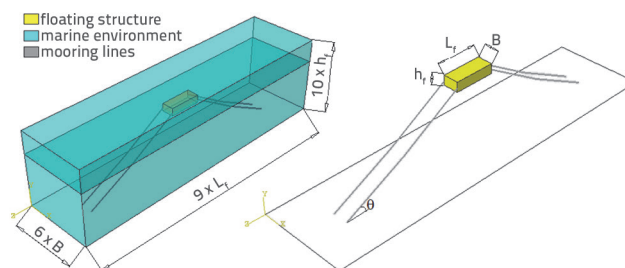


**Figure 1. Coupled model and dimensions**

### 2.1. Structural model

The numerical analysis of the floating pontoon was performed to determine the motions of the model and the tensions in the anchor chains under different wave loading conditions. The structure and the environment are depicted on the left part of Figure 1, and a schematic view of the structure with the geometrical parameters are shown on the right part. Geometrical properties are the height of the pontoon, width of the pontoon, length of the pontoon, draft of the structure, and maximum slack of the structure, which are symbolised by  $h_p$ ,  $B$ ,  $L_p$ ,  $h_d$ , and  $s$ , respectively. Further, the properties of the mooring lines are the inclination angle ( $\theta$ ), length of the mooring line ( $l$ ), radius of circular cross section ( $r$ ), and ratio of slack to taught ( $s/l$ ). The values used in the study are listed in Table 1.

The mooring lines are considered to have a Young's modulus of  $2.1 \times 10^{11}$  N/m<sup>2</sup>, density of  $8 \times 10^3$  kg/m<sup>3</sup>, and Poisson ratio of 0.3, and the average density of the floating box is 500 kg/m<sup>3</sup>. The roll moment of inertia is  $26 \times 10^3$  kgm<sup>2</sup>, yaw moment of inertia is  $146 \times 10^3$  kgm<sup>2</sup> and pitch moment of inertia is  $136 \times 10^3$  kgm<sup>2</sup>. Fully submerged inertia effects were considered for the mooring lines during the analysis.

### 2.2. Environmental model

The marine environment of the structure was modelled using the following wave parameters [36]: the wave height ( $H$ ) of 2.54 m and wave period ( $T$ ) of 7.54 s, and water depth ( $d$ ) of 18 m. The wave elevation at the point of the pontoon was simulated using two different approaches, that is, target (Case I) and induced (Case II) waves. Target wave elevation was generated using the JONSWAP wave spectrum from target values  $H = 2.5$  m and  $T = 7.54$  s. Induced wave elevation is measured at the point of the pontoon by forcing the waves, which were derived from the target wave spectrum to a numerical model. Finally, the induced wave spectrum was generated using the Fast Fourier Transform (FFT) method from

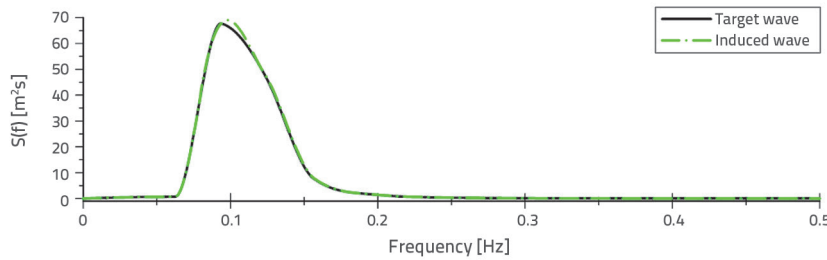


Figure 2. Target and induced wave spectra

the induced wave elevation. Thus, the pontoon is affected by two different wave cases. The power spectral density of the JONSWAP wave spectrum is given by the following equation.

$$S_{(f)} = \frac{H_s^2}{4\pi T_z^4 f^5} \exp\left(\frac{1}{\pi T_z^4 f^4}\right) \gamma \exp\left[\frac{(f-f_p)^2}{2\sigma^2 f_p^2}\right] \quad (1)$$

The target wave spectrum was generated using Eq. (1). In this equation,  $H_s$  denotes the significant wave height,  $T_z$  is the zero crossing period,  $f$  is the frequency,  $\gamma$  is the peak enhancement factor,  $f_p$  is the peak frequency, and  $\sigma$  is the width of the spectral peak. A previous study [37] showed that  $\sigma = 1.09$ ,  $f_p = 0.096 \text{ s}^{-1}$ , and  $\sigma = 0.09$ , when  $H_s = 2.54 \text{ m}$  and  $T_z$  is  $7.54 \text{ s}$ . The target wave spectrum is illustrated in Figure 2.

Multi-sinusoidal waves can be derived by using the target wave spectrum. Eqs. (2) and (3) can be used to calculate the  $H$  and  $T$  values of each individual regular wave based on the power spectral density and  $f$  values. The height of the wave at a certain frequency can be obtained as follows.

$$H(f) = 2\sqrt{2E(f)\Delta f} \quad (2)$$

$$T = 1 / f \quad (3)$$

$H$  and  $T$  values of 20 randomly selected regular waves, among the 256 waves generated, are given in Table 2. Thus, the sea surface elevation of the target wave (Case I) is obtained by the superposition of each of the 256 sinusoidal

waves. Target wave elevation can be obtained using Eq. (4), using the  $H$ ,  $T$ , and length ( $L$ ) values of each sinusoidal wave. The equation describing the free surface as a function of time  $t$  and horizontal distance  $z$  for a simple sinusoidal wave is written as follows:

$$\eta = \frac{H}{2} \cos\left(\frac{2\pi z}{L} - \frac{2\pi t}{T}\right) \quad (4)$$

Free surface elevations of the induced wave were achieved by forcing the 256 waves into the numerical domain; the use of the CEL technique suppresses free surface elevations in the Eulerian part. The elevation is evaluated at the point of the pontoon, at the Eulerian part without floating object. Although different wave theories yield different periods and heights for the multi-sinusoidal waves, they can also be modelled by considering the Airy wave theory, as reported by Chakrabarti [38].

The power spectral density  $S(f)$  of the induced wave was obtained directly from a continuous time series of the wave elevation  $\eta(t)$  by using Fourier analysis, as shown in Figure 3. The FFT method is adopted in Fourier analysis via the signal processing toolbox in MATLAB [39]. The power spectral density of the induced wave can be computed as

$$S(f) = \frac{1}{T_r} \left[ \sum_{n=0}^N \eta(n\Delta t) e^{2\pi i f n \Delta t} \Delta t \right] \quad (5)$$

The record length is represented by  $T_r$ , and the sampling interval is denoted by  $\Delta t$ . Consistency between the induced wave and the target wave can be observed in Figures 2 and 3. By determining

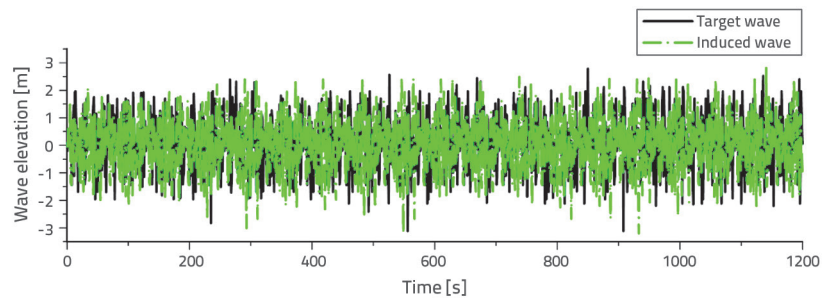


Figure 3. Target and induced wave elevation

Table 2. Wave heights and periods

Number	1	2	3	4	5	6	7	8	9	10
Wave height [m]	0.32	0.37	0.42	0.52	0.39	0.35	0.32	0.48	0.59	0.82
Wave period [s]	32.00	16.00	12.80	11.64	10.66	8.53	8.00	7.53	6.39	6.09
Number	11	12	13	14	15	16	17	18	19	20
Wave height [m]	1.22	1.55	1.38	1.24	1.06	1.02	0.76	0.59	0.35	0.27
Wave period [s]	5.56	5.33	4.92	4.57	4.00	3.55	3.20	2.90	2.28	2.00

the geometrical and physical conditions of the structure and its environment, the Lagrangian model of the structure and the Eulerian model for the marine environment were realised in the CEL model.

### 3. FSI analysis

FSI analysis of the moored pontoon-type offshore structure was performed using Abaqus [28]. In the numerical analysis, Lagrangian and Eulerian procedures were followed using the CEL technique. The mathematical definition of this technique is presented in the following sections.

#### 3.1. Mathematical definition of CEL technique

The formulation of the CEL technique used by Abaqus is described by Eqs. (6–12). Here, Eqs. (6–8) are the Lagrangian mass, momentum, and energy conservation equations, respectively.

$$\frac{D\rho}{Dt} + \rho \nabla \cdot \mathbf{v} = 0 \tag{6}$$

$$\rho \frac{D\mathbf{v}}{Dt} = \nabla \cdot \boldsymbol{\sigma} + \rho \mathbf{b} \tag{7}$$

$$\frac{De}{Dt} = \boldsymbol{\sigma} : \mathbf{D} \tag{8}$$

In the Eqs. (6–8), material velocity, density, the Cauchy stress, the body force, and the internal energy per unit volume are represented by  $\mathbf{v}$ ,  $\rho$ ,  $\boldsymbol{\sigma}$ ,  $\mathbf{b}$  and  $e$ , respectively.

$$\frac{D\phi}{Dt} = \frac{\partial \phi}{\partial t} + \mathbf{v} \cdot (\nabla \phi) \tag{9}$$

Using Eq. (9), the governing equations for the Lagrangian technique are determined in the general conservation form for Eulerian procedure as follows:

$$\frac{\partial \phi}{\partial t} + \nabla \cdot \Phi = \mathbf{S} \tag{10}$$

$\phi$  is the arbitrary solution variable,  $\Phi$  is the flux function, and  $\mathbf{S}$  is the source term in the Eq. (10). This equation can be written as two separate equations as follows:

$$\frac{\partial \phi}{\partial t} = \mathbf{S} \tag{11}$$

$$\frac{\partial \phi}{\partial t} + \nabla \cdot \Phi = 0 \tag{12}$$

Eq. (11) is therefore the same as with the standard Lagrangian formulation in the case wherein the spatial time derivative is changed to the material time derivative on the fixed mesh. The deformed mesh is transferred to the original fixed mesh. Thereafter, the volume of the material that is transferred between the adjacent elements is computed to solve the Eq. (12). Variables of the Lagrangian formulation, such as momentum, mass, stress, and energy, are then arranged to describe the material flow between the adjacent elements according to the transport algorithms.

#### 3.2. CEL application to mentioned model

Figure 4 depicts the finite element model of the structure and the marine environment. The marine environment constituting the Eulerian part and the composite structure generating the Lagrangian part are on the right part of the figure. The Eulerian part is composed of void parts with and without assigned material, as can be seen in the figure. The CEL approach enables the inclusion of various materials (including voids) in the single element. The flowing material along the mesh is followed by the Eulerian volume fractions (EVFs), symbolising the ratio as the material is filled with the Eulerian elements. If a material entirely fills the element, the EVF is equal to 1; if there is no material in the element, the EVF is considered as 0.

After generating Eulerian and Lagrangian parts in the software, material characteristics are defined for these parts. Material properties of the Lagrangian part have been given in Section 2.1. The environment of the structure is modelled as EOS materials with the velocity of sound ( $c_0$ ) in salty water at 1560 m/s, with the density ( $\rho$ ) of 1025 kg/m<sup>3</sup> and the dynamic viscosity ( $\mu$ ) of 0.0015 Ns/m<sup>2</sup>. In the model, void depth is 2 m and water depth ( $d$ ) is 18 m. The loading case and boundary conditions are defined in the next step of the numerical analysis. The direction of flow belonging to the Eulerian part is depicted in Figure 4. While target elevation is defined as the inlet for Case I, induced elevation has been defined for Case II. An outlet boundary condition is stated on the opposite side of the inlet. The bottom of the marine region is set to a wall boundary condition where all of the velocity components are equal to zero. The far field boundary condition is applied to side walls with a velocity equal

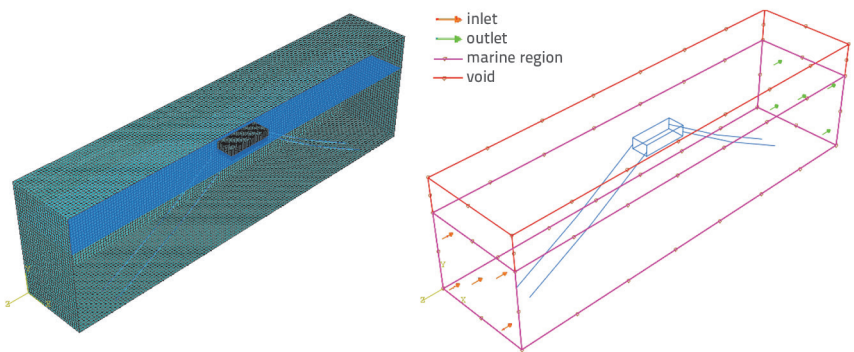


Figure 4. Mesh structure and schematic representation of the model

to their inlet velocity. Far field boundaries are transmissible such that flow is not affected by the presence of the structure at these boundaries.

### 3.2.1. Mesh design

The number of nodes and elements change due to seed sizes. Several trials have been conducted to determine the most suitable seed size through natural frequency values in the software via the Lanczos procedure. The structural eigenvalue problem has attracted great interest since the advent of finite element models. The Lanczos method is considered a significant procedure for eigenvalue problems. The Lanczos method that utilises the Householder and Q-R algorithms for the reduced eigenproblem has been implemented in the software. The Lanczos procedure in the software arises from a group of Lanczos "runs," in each of which a group of iterations called steps is generated. For each Lanczos run, the following spectral transformation, Eq. (13) is applied to Eq. (14) in which  $k$  and  $m$  are stiffness and mass matrixes, respectively. Besides,  $\theta$  represents the square of natural frequency,  $\sigma$  is the shift,  $\theta$  symbolises the eigenvalue, and  $\xi$  is the eigenvector [30]. This transformation permits swift convergence to the desired eigenvalues. It is also known that researchers utilise the Lanczos procedure for a similar purpose [27, 40].

$$[m]([k] - \sigma[m])^{-1}[m]\{\xi\} = \theta[m]\{\xi\} \tag{13}$$

$$(-\lambda[m] + [k])\{\xi\} = 0 \tag{14}$$

As indicated by Figure 4, three dimensional, 8-node linear brick, hexahedron element type (C3D8R) and linear line elements of type B31 that are suitable for the CEL technique are utilised in the modelling phase. Natural frequencies of sway mode values for different numbers of nodes and elements are given in Table 3.

Table 3 shows different values of the number of nodes and elements after sensitivity analysis. When the value of seed size is decreased from 0.075 to 0.025, the difference between natural frequency values is obtained as 4.33%. For this reason, the seed size is decided at 0.075 m in the end for the Lagrangian part. Thus, a total of 125480 nodes and

a total of 117056 elements have been used. Among these elements, B31 type 1496 belongs to the mooring line and C3D8R type 115560 belongs to the structure. On the other hand, 1708857 nodes and 1658880 EC3D8R type numbers of elements with seed sizes of 0.075 m and 0.25 m are utilised in the marine environment. While the seed size is 0.075 m in the contact points between the environment and the structure, it is 0.25 m in the rest of the environmental model.

### 3.2.2. Solution method

The CEL technique is widely used in the solution of fluid-structure interaction problems with large deformations. Eulerian analysis is an effective method for applications involving extreme deformations and including fluid flow. In these applications, traditional Lagrangian elements become highly distorted and lose accuracy. Eulerian-Lagrangian contact allows the Eulerian materials to be combined with traditional non-linear Lagrangian analysis. The contacts between the two domains have been discretised using the general contact algorithm based on the penalty contact method. Explicit analysis in which the values are transferred to fluid by the CEL technique is used to determine displacement values according to Eq. (15).

$$m^{NJ} \ddot{Z}^N |_t = (F^J - I^J) |_t \tag{15}$$

In the equation,  $m^{NJ}$  is the mass matrix,  $\ddot{Z}$  represents the acceleration,  $t$  means the time,  $F^J$  symbolizes the external applied load vector transferred from fluid flow and  $I^J$  is the internal force vector which is occurred by stresses in the elements. Finite element analysis is performed with a 0.01 sec time step ( $\Delta t$ ) for 600 sec. The equations of motion for the body are integrated due to equations given below for Explicit rule.

$$\dot{Z}^N_{(i+\frac{1}{2})} = \dot{Z}^N_{(i-\frac{1}{2})} + \frac{\Delta t_{(i+1)} + \Delta t_{(i)}}{2} \ddot{Z}^N_i \tag{16}$$

$$Z^N_{(i+1)} = Z^N_{(i)} + \Delta t_{(i+1)} \dot{Z}^N_{(i+\frac{1}{2})} \tag{17}$$

Table 3 Mesh size sensitivity analysis results

Seed size [m]	Node number	Element number		Natural frequency [rad/s]	Change between to rows [%]
		Mooring lines	Floating structure		
0.15	16624	748	13780	0.550	17.02
0.10	53851	1120	48000	0.470	14.91
0.075	125480	1496	115560	0.409	3.28
0.05	404901	2240	384000	0.396	1.02
0.025	3150605	4484	3072000	0.392	

$$\ddot{Z}_{(i)}^N = (m^{NJ})^{-1} (F_i^J - I_i^J) \tag{18}$$

$Z^N$ ,  $\dot{Z}^N$  and  $\ddot{Z}^N$  are degree of freedom, (N) of displacement, velocity and acceleration components respectively. Velocity and displacement values can be obtained after determining accelerations. Validation of the numerical model is checked via free surface elevations. As the CEL technique prevents obtaining free surface elevation of the Eulerian part, the output of the analysis is compared with the analytical results of Eq. (4).

### 4. Results

First of all, the wave elevation of the wave ( $H = 2.54$ ,  $T = 7.54$  s) is obtained and compared with analytical results as it is in Figure 5.

At the entry point of the model for  $z = 0$  position, the wave elevation that is analytically obtained oscillates between the range of  $-1.25$  m and  $+1.25$  m. Numerical values for the same position range between  $-1.34$  m and  $+1.35$  m. On the other hand, while the elevation for the  $z = 36$  m position is analytically varies between  $-1.25$  m and  $+1.25$  m, the elevation for the same position is numerically changed between  $-1.31$  m and  $+1.32$  m. For  $z = 72$  m position, which is the exit point of the model, analytical values oscillate between the same values as in case of the other positions. However, numerical values are between  $-1.33$  m and  $+1.33$  for this position. The maximum difference occurs at 8% between the numerical and analytical results at  $z = 0$  position.

Heave, surge, and pitch motions of the structure and maximum tension of the mooring lines are comparatively obtained according to Case I and Case II, and they are given in Figure 6. The vertical motion of the model is greater due to the fluctuations of water slope and vertical wave force. The wave effects the structure axially. Lateral motion in this direction is restrained by mooring lines in this direction. On the other hand, the limited motion is derived from drooping modelled mooring lines. As the wave does not affect the structure angularly, translational movement can be ignored in the  $x$  direction. Angular motion is observed due to pitch motion in the wave direction. Because the wave does not angularly affect the structure and symmetrical mooring lines are used in the four corners of the structure, angular motion is not taken into consideration in the other directions.

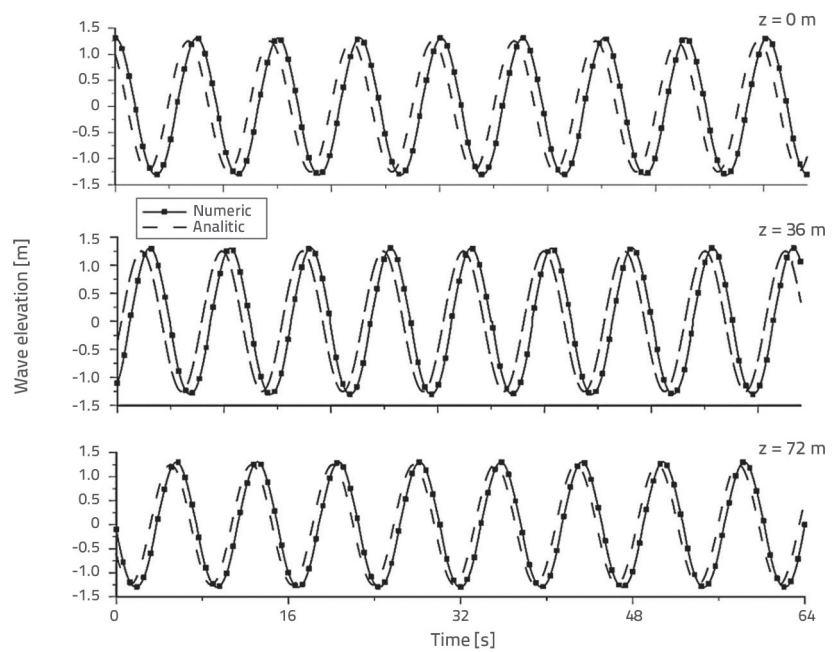


Figure 5. Wave elevations

Table 4. Statistical values of structural outputs

Outputs \ Values	Heave [m]		Surge [m]		Pitch [°]		Tension [N]	
	Case I	Case II	Case I	Case II	Case I	Case II	Case I	Case II
Minimum	-0.53	-0.56	-0.026	-0.029	-4.36	-5.02	$3.69 \times 10^5$	4.04
Maximum	+0.82	0.88	0.058	0.062	6.30	6.81	$5.13 \times 10^5$	5.59
Mean	0.116	0.123	0.013	0.016	1.490	1.607	$4.37 \times 10^5$	4.76
Standard deviation	0.427	0.454	0.027	0.030	3.50	3.762	$4.63 \times 10^4$	5.04

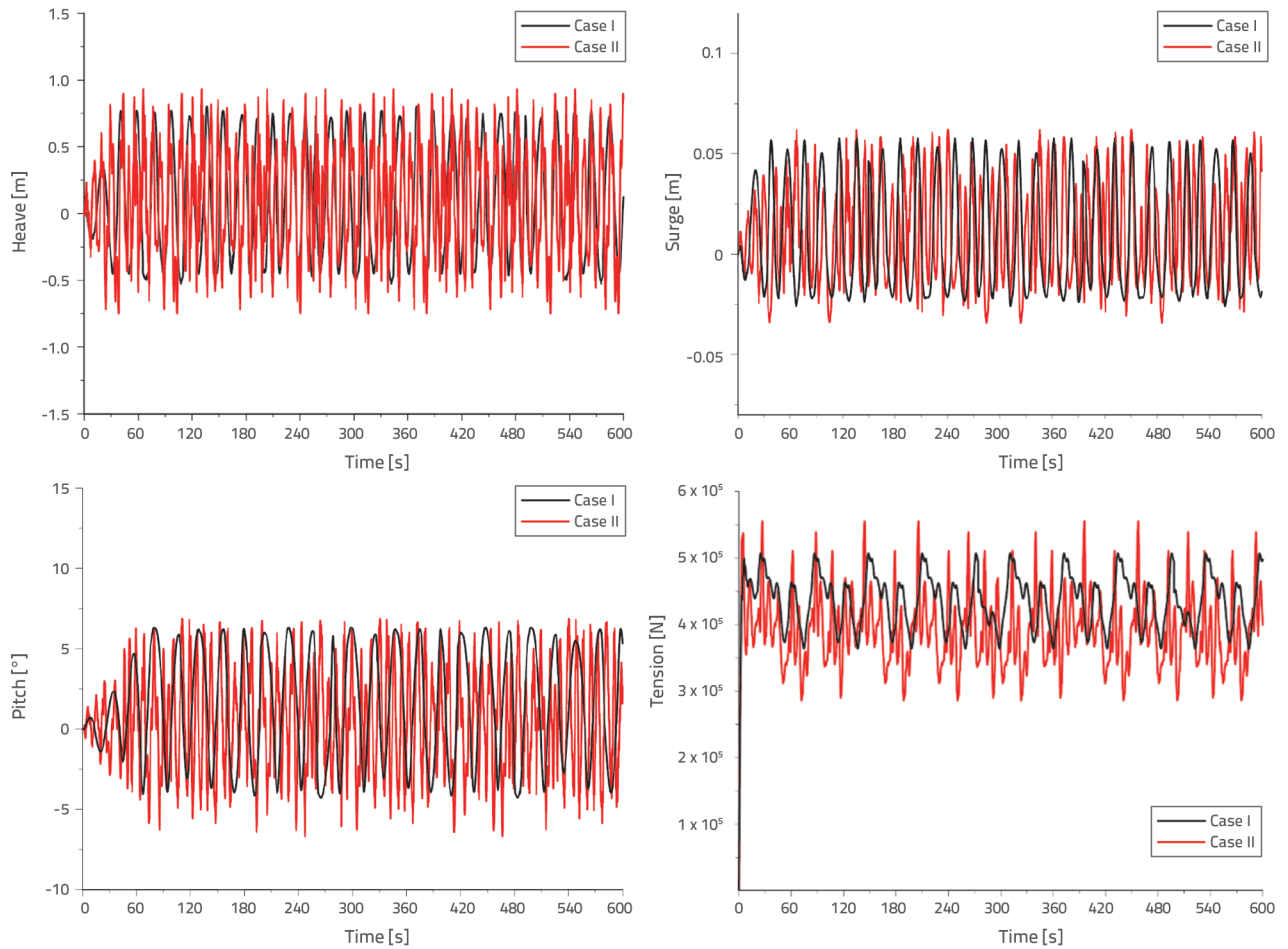


Figure 6. Time histories of motions of the structure and maximum tension of the mooring lines

Statistical values of heave, surge, pitch motions, and tensions of the mooring lines are given in Table 4.

The mode shapes of the structure and the corresponding natural frequency values are obtained by numerical analysis via the Lanczos Method. The results are given in Table 5.

The dominant modes of such structures emerge from modal analysis. In addition, natural frequency values increase starting from the first mode as expected. While sway, heave, and surge motions are obtained as translational motions, roll,

pitch, and yaw motions are obtained as rotational motions due to the visual results of modal behaviour. The shapes of the six modes of the structure are visually presented in Figure 7. While translational displacements are in metres, rotational displacements are in degrees in the following figure.

Coupled motions of the system are given in Figure 8 for both cases. The simulation result for Case I is provided in the left part of the figure, and that for Case II is depicted in the right part of the figure for different time periods.

Table 5. Natural frequencies and corresponding mode shapes

Outputs \ Modes	1	2	3	4	5	6
Mode shape	Sway	Pitch	Yaw	Heave	Roll	Surge
Natural frequency [rad/s]	0.409	0.468	1.129	1.381	1.489	2.105

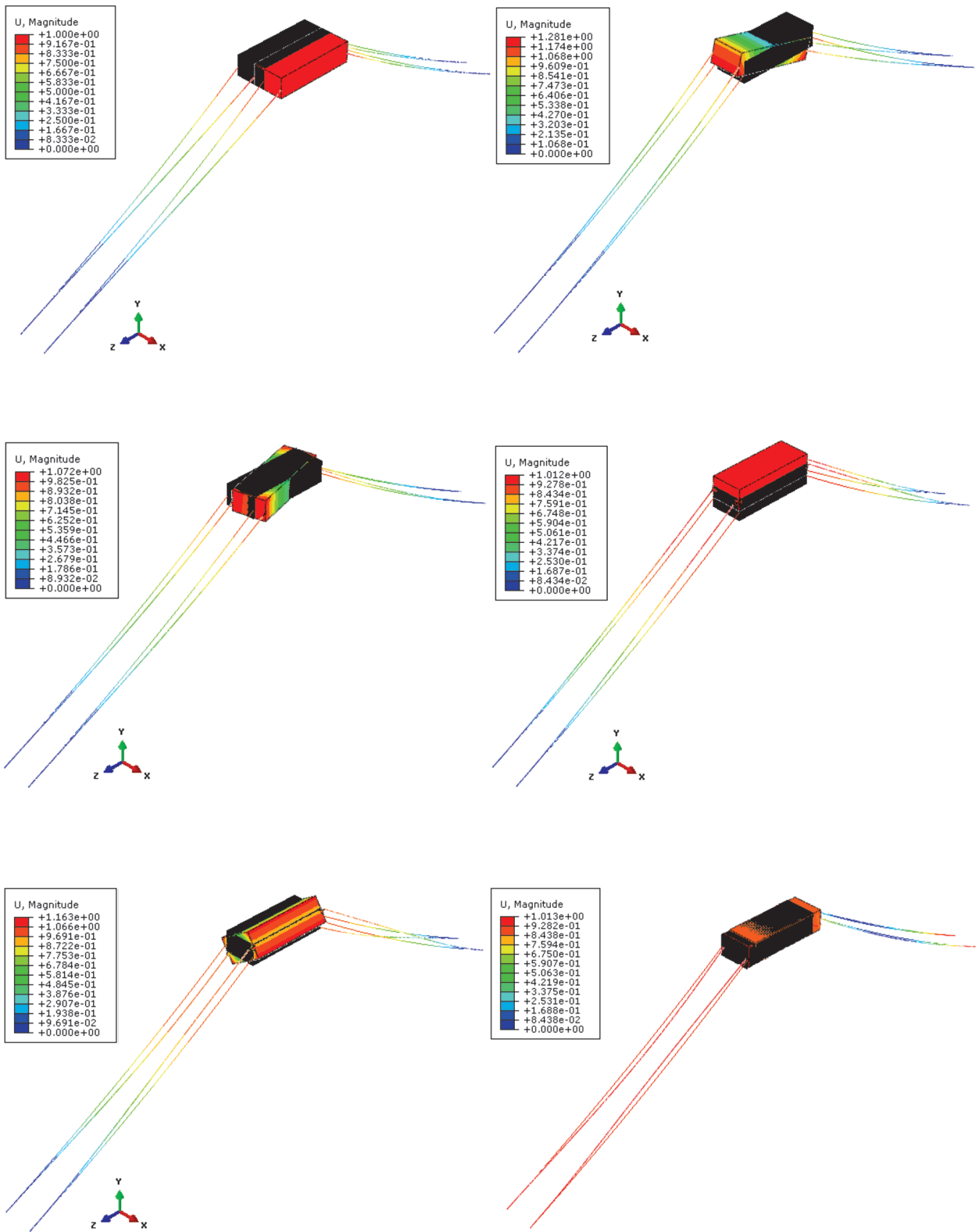


Figure 7. Mode shapes and corresponding natural frequencies of the structure

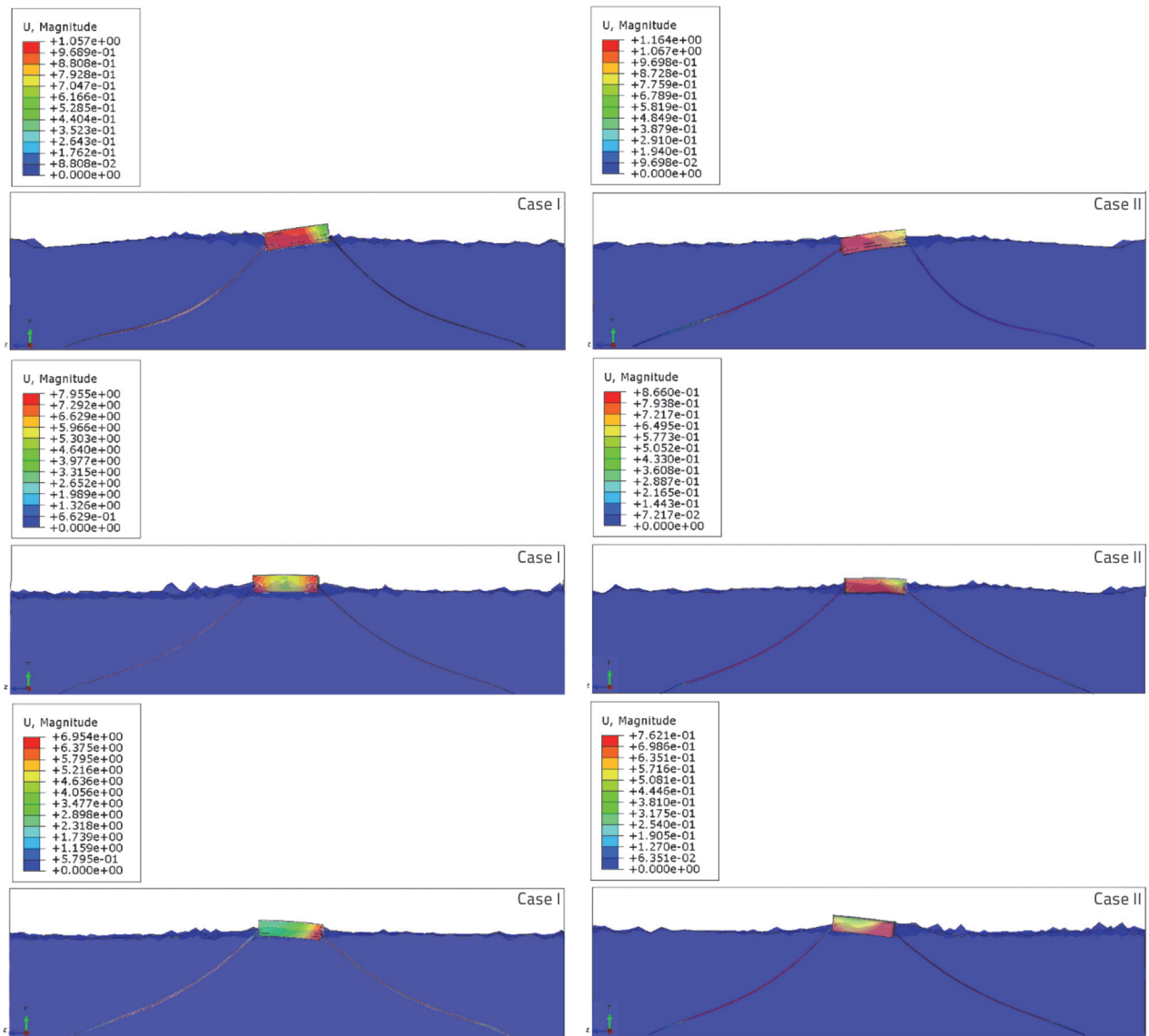


Figure 8. Coupled motions of the mooring lines, floating structure and marine environment

### 5. Conclusion

Use of these structures has become prevalent as floating structures can be utilised at any depth. Unlike the structures that are directly fixed to the sea bottom, floating structures are not affected by different water depths and effects of the sea bottom. However, their thickness is much smaller than their surface value. For this reason, while stretching and bending effects may occur under wave force, sudden translations may be observed under windstorms. Therefore, the marine environment should be realistically modelled in the design phase so as not to encounter these negative effects. In the scope of this study, the marine environment is modelled by different wave loading conditions to reveal the differences between the two cases. The wave model that constitutes the flow environment is generated by the Eulerian procedure. On the other hand, the structure is

modelled by the Lagrangian procedure. The interaction of these two environments is provided by the CEL technique. Numerical analysis is performed on wave surface profile in the first place. Eulerian procedure that allows movement of free water has been utilised in the modelling of the marine environment. Besides, free surface movement of the Eulerian part is analytically obtained by the equation of surface profile belonging to linear wave theory. The maximum difference between numerical and analytical results is determined as 8.5%. Therefore, the accordance of water surface profiles has been verified. Only wave models are generated without placing the structure in the validation phase of wave profiles. Water surface profiles are obtained for the determined two points. It is considered that the numerical comparison with the analytical method would not give reliable results due to the deterioration of the flow structure when the structure is placed inside.

Heave, surge, and pitch motions of the structure are comparatively obtained according to Case I and Case II. The maximum difference between these two cases is 7.92%, 7.13%, and 8.46% according to heave, surge, and pitch motions. Furthermore, the difference between the cases is determined as 9.42% according to the maximum mooring line tension value. When these differences are investigated, it is determined that more critical results are obtained for Case II. Coupled motions of the mooring lines, floating structure and marine environment have been visually presented in Figure 8. In this situation, the total displacement of the floating structure for Case I is obtained as 10.11% bigger than for Case II.

After numerical analysis, the first six modes and related frequency values are obtained. While heave motions are obtained as translational motions, roll, pitch, and yaw motions are obtained as rotational motions due to the visual results of modal behaviour. Sensitivity analysis is performed through modal analysis. It is well known that the number of nodes and elements has a significant effect on the numerical results and computation time of the analysis. Thus, the most suitable node and element numbers are decided in the first place. C3D8R typed elements have been utilised for the structure. On the other hand, EC3D8R typed elements having the same properties as C3D8R typed elements are used for the fluid. The numbers of nodes and elements have been given in Table 3. If the physical problem is solved by only the Lagrangian procedure instead of the Eulerian–Lagrangian procedure, the element type will be C3D10M. Besides, when the seed size remains constant, 660171 nodes and 471446 elements in the structure and mooring line will be used. Aside from the increased number of nodes and elements, the structure and fluid will be modelled

in various interfaces. The interaction between the interfaces will be provided through contact surfaces.

Solution time extends and high performance computer technology is required to perform numerical analysis due to different interfaces and an increase in the number of nodes and elements. For this reason, analysis results are obtained faster when Eulerian–Lagrangian approaches are utilised together in the fluid–structure interaction problems. It is also known that association of these approaches gives more reliable results in interaction analysis where big deformations occur.

The effects of different wave models on the structural behaviour of the floating structure are determined in this study. These effects prominently appear in heave, surge, and pitch motions when the wave effects pass through the axis of the structure. It is aimed to investigate the behaviour of sway, yaw, and roll motions under the effect of different wave models by changing the incidence angle of the wave in further studies. Furthermore, it is suggested that the effect of changing multi-sinus wave numbers on structural behaviour be investigated.

As a conclusion, it is stated that Case II, in which surface elevation is obtained from a numerical model, is more critical than Case I, in which surface elevation is obtained from the equation of free surface. Therefore, bigger motion values have appeared on the structure due to Case II. The same behaviour is also observed in the stress values of floating members. It is also concluded that the design of the floating structure by Case II gives more reliable results due to the CEL technique enabling free surface modelling. It is thought that this study will shed light on further studies investigating the numerical behaviour of pontoon-type structures under the effect of various load conditions by different procedures.

## REFERENCES

- [1] Xu, S., Murai, M., Wang, X., Takahashi, K.: A novel conceptual design of a dynamically positioned floating wind turbine, *Ocean Engineering*, 221 (2021), <https://doi.org/10.1016/j.oceaneng.2020.108528>.
- [2] Ji, C.Y., Chen, X., Cui, J., Gaidai, O., Incecik, A.: Experimental study on configuration optimization of floating breakwaters, *Ocean Engineering*, 117 (2016), pp. 302–310. <https://doi.org/10.1016/j.oceaneng.2016.03.002>.
- [3] Liu, Z., Wang, Y.: Numerical investigations and optimizations of typical submerged box-type floating breakwaters using SPH, *Ocean Engineering*, 209 (2020), <https://doi.org/10.1016/j.oceaneng.2020.107475>.
- [4] Gomes, R.P.F., Gato, L.M.C., Henriques, J.C.C., Portillo, J.C.C., Howey, B.D., Collins, K.M., Hann, M.R., Greaves, D.M.: Compact floating wave energy converters arrays: Mooring loads and survivability through scale physical modelling, *Applied Energy*, 280 (2020), <https://doi.org/10.1016/j.apenergy.2020.115982>.
- [5] Chandrasekaran, S., Sricharan, V.V.S.: Numerical analysis of a new multi-body floating wave energy converter with a linear power take-off system, *Renewable Energy*, 159 (2020), pp. 250–271. <https://doi.org/10.1016/j.renene.2020.06.007>.
- [6] Tang, H.J., Huang, C.C., Chen, W.M.: Dynamics of dual pontoon floating structure for cage aquaculture in a two-dimensional numerical wave tank, *Journal of Fluids and Structures*, 27 (2011), pp. 918–936. <https://doi.org/10.1016/j.jfluidstructs.2011.06.009>.
- [7] Viuffa, T., Xiang, X., Øiseth, O., Leira, B.J.: Model uncertainty assessment for wave- and current-induced global response of a curved floating pontoon bridge, *Applied Ocean Research*, 105 (2020), <https://doi.org/10.1016/j.apor.2020.102368>.
- [8] Aboshio, A., Ye, J.: Numerical study of the dynamic response of Infiatable Offshore Fender Barrier Structures using the Coupled Eulerian–Lagrangian discretization technique, *Ocean Engineering*, 112 (2016), pp. 265–<https://doi.org/10.1016/j.oceaneng.2015.12.020>.
- [9] Gao, R.P., Wang, C.M., Koh, C.G.: Reducing hydroelastic response of pontoon-type very large floating structures using flexible connector and gill cells, *Engineering Structures*, 52 (2013), pp. 372–383. <https://doi.org/10.1016/j.engstruct.2013.03.002>.
- [10] Loukogeorgaki, E., Yagci, O., Kabdasi, M.S.: 3D Experimental investigation of the structural response and the effectiveness of a moored floating breakwater with flexibly connected modules, *Coastal Engineering*, 91 (2014), pp. 164–180, <https://doi.org/10.1016/j.coastaleng.2014.05.008>.

- [11] Chuang, Z., Chang, X., Li, C., Lu, Y., Liu, S.: Performance change of a semi-submersible production platform system with broken mooring line or riser, *Engineering Failure Analysis*, 118 (2020), <https://doi.org/10.1016/j.engfailanal.2020.104819>.
- [12] Lim, D.H., Kim, Y.: Design wave method for the extreme horizontal slow-drift motion of moored floating platforms, *Applied Ocean Research*, 71 (2018), pp. 48–58, <https://doi.org/10.1016/j.apor.2017.12.004>.
- [13] Cheng, Y., Ji, C., Zhai, G., Gaidai, O.: Hydroelastic analysis of oblique irregular waves with a pontoon-type VLFS edged with dual inclined perforated plates, *Marine Structures*, 49 (2016), pp. 31–57, <https://doi.org/10.1016/j.marstruc.2016.05.008>.
- [14] Trubat, P., Molins, C., Gironella, X.: Wave hydrodynamic forces over mooring lines on floating offshore wind turbines, *Ocean Engineering*, 195 (2020), <https://doi.org/10.1016/j.oceaneng.2019.106730>.
- [15] Jin, C., Bakti, F.P., Kim, M.H.: Multi-floater-mooring coupled time-domain hydro-elastic analysis in regular and irregular waves, *Applied Ocean Research*, 101 (2020), <https://doi.org/10.1016/j.apor.2020.102276>.
- [16] Howe, D., Nader, J.R., Macfarlane, G.: Performance analysis of a floating breakwater integrated with multiple oscillating water column wave energy converters in regular and irregular seas, *Applied Ocean Research*, 99 (2020), <https://doi.org/10.1016/j.apor.2020.102147>.
- [17] Yuan, Z.M., Incecik, A., Ji, C.: Numerical study on a hybrid mooring system with clump weights and buoys, *Ocean Engineering*, 88 (2014), pp. 1–11, <https://doi.org/10.1016/j.oceaneng.2014.06.002>.
- [18] Chung, W.C., Kang, H.Y., Kim, M.H.: Multi-scale approach for chain-mooring OPB-induced failure considering time-varying interlink bending stiffness and fairlead condition, *Applied Ocean Research*, 98 (2020), <https://doi.org/10.1016/j.apor.2020.102128>.
- [19] Qiao, D., Yan, J., Liang, H., Ning, D., Li, B., Ou, J.: Analysis on snap load characteristics of mooring line in slack-taut process, *Ocean Engineering*, 196 (2020), <https://doi.org/10.1016/j.oceaneng.2019.106807>.
- [20] Wiegard, B., Radtke, L., König, M., Moustafa, A. M., Düster, A.: Simulation of the fluid-structure interaction of a floating wind turbine, *Ships and Offshore Structures*, 14 (2019), pp. 207–218, <https://doi.org/10.1080/17445302.2019.1565295>.
- [21] Chen, X., Miao, Y., Tang, X., Liu, J.: Numerical and experimental analysis of a moored pontoon under regular wave in water of finite depth, *Ships and Offshore Structures*, 12 (2017) 3, pp. 412–423, <https://doi.org/10.1080/17445302.2016.1172831>.
- [22] Ji, C., Cheng, Y., Yang, K., Oleg, G.: Numerical and experimental investigation of hydrodynamic performance of a cylindrical dual pontoon-net floating breakwater, *Coastal Engineering*, 129 (2017), pp. 1–16, <https://doi.org/10.1016/j.coastaleng.2017.08.013>.
- [23] Martínez, E.L., Quiroga, A.G., Jardini, A.L., Filho, R.M.: Computational fluid dynamics simulation of the water – sugar cane bagasse suspension in pipe with internal static mixer, *Computer Aided Chemical Engineering*, 26 (2009), pp. 683–688, [https://doi.org/10.1016/S1570-7946\(09\)70114-2](https://doi.org/10.1016/S1570-7946(09)70114-2).
- [24] Gücüyen, E., Erdem, R.T., Gökkuş, Ü.: FSI analysis of submarine outfall, *Brodogradnja/Shipbuilding*, 67 (2016) 2, pp. 67–80, <https://doi.org/10.21278/brod67205>.
- [25] Korobenko, A., Yan, J., Gohari, S. M.I., Sarkar, S., Bazilevs, Y.: FSI Simulation of two back-to-back wind turbines in atmospheric boundary layer flow, *Computers and Fluids*, 158 (2017), pp. 167–175, <https://doi.org/10.1016/j.compfluid.2017.05.010>.
- [26] Liu, J.: A second-order changing-connectivity ALE scheme and its application to FSI with large convection of fluids and near contact of structures, *Journal of Computational Physics*, 304 (2016), pp. 380–423, <https://doi.org/10.1016/j.jcp.2015.10.015>.
- [27] Gücüyen, E., Yiğit, M.E., Erdem, R.T., Gökkuş, Ü.: Comparative analysis of tripod offshore structure, *Građevinar*, 72 (2020) 11, pp. 1021–1030, <https://doi.org/10.14256/JCE.2848.2019>.
- [28] ABAQUS User's Manual, Version 6.12, SIMULIA, Dassault Systèmes Simulia Corp., 2015.
- [29] Aquelet, N., Souli, M., Olovsson, L.: Euler–Lagrange coupling with damping effects: application to slamming problems, *Computer Methods in Applied Mechanics and Engineering*, 195 (2006), pp. 110–132, <https://doi.org/10.1016/j.cma.2005.01.010>.
- [30] ABAQUS Documentation, Version 6.12. SIMULIA, Dassault Systèmes Simulia Corp., 2015.
- [31] Ducobu, F., Riviere-Lorphevre, E., Filippi, E.: Application of the Coupled Eulerian-Lagrangian (CEL) method to the modeling of orthogonal cutting, *European Journal of Mechanics A/ Solids*, 59 (2016), pp. 58–66, <https://doi.org/10.1016/j.euromechsol.2016.03.008>.
- [32] Ning, D. Z., Zhao, X. L., Zhao, M., Hann, M., Kang, H.G.: Analytical investigation of hydrodynamic performance of a dual pontoon WEC-type breakwater, *Applied Ocean Research*, 65 (2017), pp. 102–111, <https://doi.org/10.1016/j.apor.2017.03.012>.
- [33] Zhan, J.M., Chen, X.B., Gong, Y.J., Hu, W.Q.: Numerical investigation of the interaction between an inverse T-type fixed/ floating breakwater and regular/irregular waves, *Ocean Engineering*, 137 (2017), pp. 110–119, <https://doi.org/10.1016/j.oceaneng.2017.03.058>.
- [34] Haicheng, Z., Daolin, X., Huai, Z., Shuyan, X., Yousheng, W.: Energy extraction of wave energy converters embedded in a very large modularized floating platform, *Energy*, 158 (2018), pp. 317–329, <https://doi.org/10.1016/j.energy.2018.06.031>.
- [35] Ji, C., Cheng, Y., Cui, J., Yuan, Z., Gaidai, O.: Hydrodynamic performance of floating breakwaters in long wave regime: An experimental study, *Ocean Engineering*, 152 (2018), pp. 154–166, <https://doi.org/10.1016/j.oceaneng.2018.01.055>.
- [36] Gücüyen, E., Erdem, R. T., Gökkuş, Ü.: Irregular wave effects on dynamic behaviour of piles, *Arabian Journal for Science and Engineering*, 38 (2013) 5, pp. 1047–1057, <https://doi.org/10.1007/s13369-012-0428-6>.
- [37] Houmb, O.G., Overvik, T., Parameterization of wave spectra and long term joint distribution of wave height and period, *Behaviour Of Off-Shore Structures Proceedings Of The First International Conference VOLUME ONE*, August 2nd - 5th 1976
- [38] Chakrabarti, S.: *Handbook of Offshore Engineering*, Elsevier Ltd, 2005.
- [39] Matlab Users Manuel, Version 6.5, The MathWorks, Inc, 2006.
- [40] Coutinho, A.L.G.A., Alves, J.L.D., Landau, L., Prates de Lima, E.C.: On the application of an element-by-element Lanczos solver to large offshore structural engineering problems, *Computers & Structures*, 27 (1987) 1, pp. 27–37, [https://doi.org/10.1016/0045-7949\(87\)90179-9](https://doi.org/10.1016/0045-7949(87)90179-9).